Thermal characterization of Ge-rich GST/TiN thin multilayers for phase change memories

Clément Chassain, Andrzej Kusiak, Cécile Gaborieau, Yannick Anguy, Nguyet-Phuong Tran, Chiara Sabbione, Marie-Claire Cyrille, Claudia Wiemer, Alessio Lamperti, Jean-Luc Battaglia

Thermal characterization of Ge-rich GST/TiN thin multilayers for phase change memories

Clément Chassain[1],* Andrzej Kusiak[1], Cécile Gaborieau[1], Yannick Anguy[1], Nguyet-Phuong Tran[2], Chiara Sabbione[2], Marie-Claire Cyrille[2], Claudia Wiemer[3], Alessio Lamperti[3], and Jean-Luc Battaglia[1]
[1]*I2M Laboratory Bordeaux University,* [2]*CEA LETI,* [3]*IMM-CNR*

In the domain of phase change memories (PCM), intensive research is conducted to reduce the programming cycle cost. The RESET operation is done by melting the PCM and then quenching the liquid phase to put it back to the amorphous state. In most of the devices, the heating is realized by Joule effect with a titanium nitride (TiN) component put in contact with the PCM itself. One of the crucial point to improve the efficiency of this technology is to characterize the thermal contact between the TiN and PCM. Having a low thermal resistance between the heater and the PCM ensures the heat transfer between the two is as efficient as possible. In this work the interfacial thermal resistance between Ge-doped $G_2Sb_2Te_5$ (GeGST)/TiN in multilayer systems (MLS) has been characterized and the influence of the compressive stress exerted by the TiN layers on the GeGST crystallization has been highlighted.

I. INTRODUCTION

Phase change memory (PCM) is one of the most promising technology of the next generation of non-volatile memories for storage class memory applications and neuromorphic computing [1]. In a PCM cell, the information is stored at the nanoscale through the local crystalline phase. The amorphous state is the high electrical resistance state (RESET state) while the polycrystalline state acts as the low resistance state (SET state). The memory is programmed by heating the working volume by Joule effect with different settings depending on the new state to program. One of the biggest limitations of the PCM is the high energy cost of the RESET operation. After crystallization, the return to the amorphous state is accomplished by melting (locally) the structure followed by the quench of the melted phase. Thus, reducing energy losses is a crucial aspect of PCM technological development [2, 3] . One of the approaches to reduce the power consumption of the PCM is to lower the thermal conductivity of the crystalline state, leading to a more localized heating, resulting in a more efficient raise in temperature. To fit these requirements chalcogenide alloys such as GeTe or $Ge_2Sb_2Te_5$ have been used intensively. These chalcogenide alloys are often doped with light elements (C,N,O) and/or atoms already composing them (such as Ge for example), leading to better data retention and lower RESET current [4, 5]. As the transition times for the phase change and the energy consumption have been reduced with the technological improvements, the alloy implementation went from the so-called 'mushroom' programming volume [6, 7] to nanowires [8–10] of a few nanometers in diameter or even PCM supper-lattices leading to the interfacial phase change memory technology [11]. In the case of the mushroom configuration, the heater is usually made of titanium nitride (TiN) and directly put on the programmed PCM area. Thus, it is crucial to know the interfacial thermal resistance between TiN and the PCM. A low interfacial thermal resistance is the key to avoid unnecessary heating.

In this paper the interfacial thermal resistance between Ge-doped $Ge_2Sb_2Te_5$[1] (GeGST) and TiN is characterized by modulated photothermal radiometry (MPTR) from room temperature up to 400°C. The experiments are conducted on multilayer system (MLS) composed of successive layers of TiN and GeGST stacked onto a silicon (Si) wafer.The MPTR method allows the characterization of the total thermal resistance (RTH) of the MLS, which is directly linked to the interfacial thermal boundary resistances (TBR) between GeGST and TiN layers. The MLS were created to reproduce the interface between the heater (TiN) and the PCM (GeGST) present in the mushroom configuration, thus allowing its characterization. In order to increase our experimental sensitivity to this parameter, more than one interface has been reproduced. Hence the MLS structure. It is shown that after annealing at high temperatures $TBR_{GeGST/TiN}$ tends to zero. In-situ Raman scattering analysis coupled to Tof-SIMS measurements highlightthe influence of the compressive stress exerted by the TiN layers on the GeGST layers, leading to an increase in the crystallization temperature of the GeGST.

II. EXPERIMENTAL SETUP

The schematic view of the setup is presented in Fig. 1 and is explained in details in the literature [12]. Thermal characterization is done by putting the sample in an oven working under an argon atmosphere. The sample is heated from 50°C to 400°C with a 100°C/min heat rate. The excitation source is a laser of 1064 nm wavelength and 1.7 W maximum power. The laser spot radius is

* clement.chassain@u-bordeaux.fr

[1] The deposition method ensured a 7% nitrogen (N) nominal doping of the Ge-rich GST layers as discussed later [8–10].

0.8 mm. The modulation of the laser is enabled by an opto-acoustic modulator using a squared signal coming from a function generator. The proper emission of the sample after the perturbation is collected by an infrared HgCdTe detector with a sensitive element of 0.5 mm in diameter. A lock-in amplifier is used to measure the amplitude and the phase lag ϕ between the reference and the detector output according to the frequency f. The TTL output signal from the function generator is used as the reference for the lock-in amplifier. In order to remove any bias induced by the measurement chain, a calibration was realized on an already well characterized semi infinite bulk. The phase correction regarding to the frequency is expressed as: $\phi_{real} = \phi_{exp} + 7.49 \times 10^{-4} f - 0.14$. In addition, the oven was also calibrated using an infrared camera. The true temperature T is related to the setpoint temperature T_{oven} according to: $T = 0.8685 T_{oven} + 12.24$.

III. SAMPLE PREPARATION

The GeGST/TiN MLS have been fabricated by magnetron sputtering, combining argon and nitrogen as sputtering gases. The MLS is composed of a repetition of N cells composed of 10 nm of GeGST and 10 nm of TiN as shown in Fig. 2. Two MLS thicknesses are considered namely, 100 nm ($N = 5$) and 200 nm ($N = 10$). The GeGST is obtained using co-sputtering from two stoichiometric targets, namely Ge and $Ge_2Sb_2Te_5$. The selected Ge-rich composition is referred to as "GST + Ge 45%" where 45% is the nominal fraction of Germanium added to the $Ge_2Sb_2Te_5$ reference alloy [13]. The MLS has been deposited onto a 200 mm in diameter silicon wafer (750 μm thickness) covered by a 300 nm thick S_3N_4 (SiN) passivation layer. The sputtering gas was chosen in order to ensure a 7% nitrogen (N) nominal doping of the Ge-rich GST layers [14]. The GeGST produced thereby is typified by a finer grain structure and a higher crystallization temperature than the reference GST alloy [15]. The GeGST within the MLS is deposited in the amorphous state. After deposition, the stack was coated with a 100 nm thick sputtered layer of Pt layer in order to obtain an optical to thermal transducer for the photothermal measurements. The Pt coating is also preventing the oxidation and the evaporation of the MLS at high temperature. A 10 nm thick TiN layer is deposited between the Pt and the MLS to improve the adhesion of Pt.

IV. PHYSICAL DETAILS AND MODELING

The periodic temperature variation $\Delta T(\omega)$ at the surface of the sample being small enough, it is assumed that the measured proper emission seen by the IR detector is linearly proportional to $\Delta T(\omega)$. Under the assumption of 1D heat transfer in the sample, where there is no heat loss and a semi-infinite behavior for the substrate, it has been established that [16, 17]:

$$\frac{\Delta T(\omega)}{\varphi_0(\omega)} = Z_{Si}(\omega) + RTH \tag{1}$$

where $\varphi_0(\omega)$ is the heat flux and $\omega = 2\pi f$ is the pulsation. The thermal impedance of the silicon substrate is $Z_{Si}(\omega) = 1/\left(E_{Si}\sqrt{j\,\omega}\right)$, with $E_{Si} = \sqrt{a_{Si}/k_{Si}^2}$ (a_{Si} and k_{Si} are the thermal diffusivity and thermal conductivity of the silicon wafer respectively) and $j^2 = -1$. Finally, RTH is the thermal resistance of the (Pt/TiN/MLS/SiN) stack. The phase lag $\phi(\omega)$ is calculated from (1) as :

$$\phi(\omega) = \tan^{-1}\left(\frac{-\sqrt{\frac{a_{Si}}{2\omega k_{Si}^2}}}{\sqrt{\frac{a_{Si}}{2\omega k_{Si}^2}} + RTH}\right) \tag{2}$$

Assuming the Pt and TiN layers fully thermalized at each frequency ω, the thermal resistance RTH of the stack is expressed as:

$$RTH = N\left(\frac{e_{GeGST}}{k_{GeGST}} + \frac{e_{TiN}}{k_{TiN}} + 2TBR_{GeGST/TiN}\right) + \frac{e_{SiN}}{k_{SiN}} + TCR \tag{3}$$

With:

$$TCR = TBR_{Pt/TiN} + TBR_{SiN/Si} + TBR_{TiN/SiN} \tag{4}$$

where e_i and k_i denote respectively the thickness and the thermal conductivity of layer i, N is the number of repetition of GeGST/TiN associations in the MLS and $TBR_{i/k}$ denotes the thermal boundary resistance between contiguous layers i and k. The required parameters for the calculation of RTH from relation (3) are reported in Tab. I.

It is possible to compute a theoretical value of the interfacial thermal resistance between layers using the diffuse mismatch model (DMM) [21]. The expression of the interfacial thermal resistance between materials 1 and 2 from the DMM is:

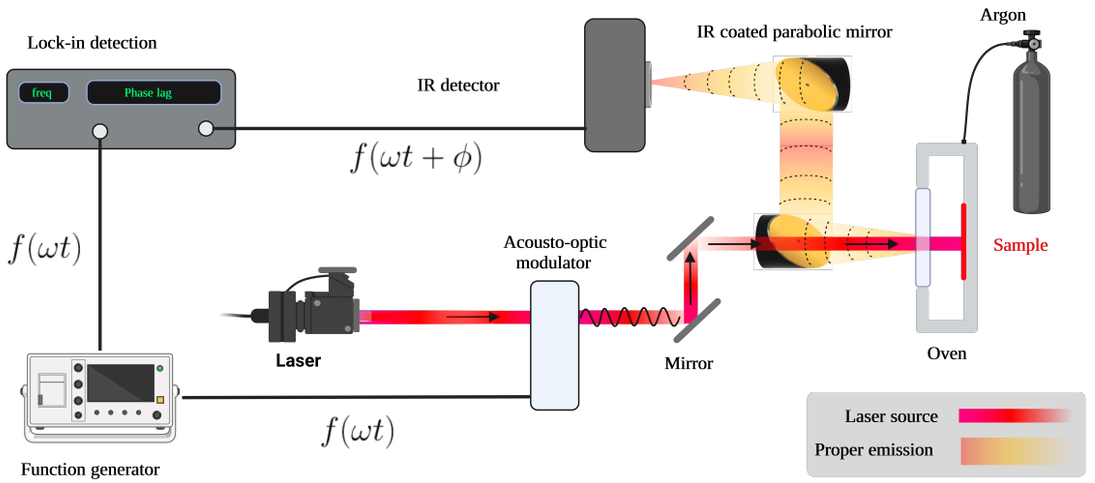

Figure 1. MPTR experimental setup. The sample is put inside a furnace that permits reaching 1200 °C under inert gas.

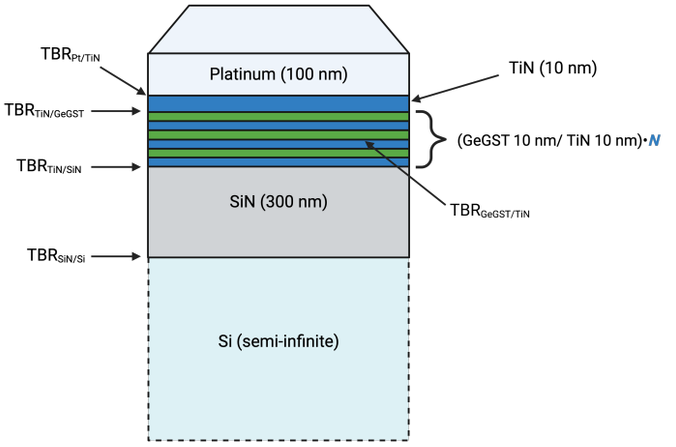

Figure 2. Schematic view of the sample composition. A Pt film is deposited to act as an optical to thermal transducer. The TiN layer improves the adhesion of Pt. The stack involves several thermal interface resistances. The sum of those thermal boundary resistances (outside of those within the MLS), is designated as TCR, with $TCR = TBR_{Pt/TiN} + TBR_{TiN/SiN} + TBR_{SiN/Si}$.

$$TBR_{1/2} = \left(\sum_j \frac{k_B^4\, T^3}{8\,\pi^2\,\hbar^3\, V_{j,1}^2} \alpha_{1\to 2} \int_0^{\Theta_{D,1}/T} \frac{x^4\, e^x}{\left(e^x - 1\right)^2} \mathrm{d}x \right)^{-1}_{j=(L,T,T)} \tag{5}$$

In this equation, $\hbar$ is the reduced Planck constant, k_B is the Boltzmann constant, V_j is the velocity of the phonons in the different directions (j=(L,T,T), L is the longitudinal direction and T are the two transversal ones) and Θ_D is the Debye temperature. The phonon transmission coefficient α is defined as [21]:

$$\alpha_{1\to 2} = \frac{v_{L,2}^{-2} + 2v_{T,2}^{-2}}{v_{L,1}^{-2} + 2v_{T,1}^{-2} + v_{L,2}^{-2} + 2v_{T,2}^{-2}} \tag{6}$$

The Levenberg-Marquardt minimization algorithm [22–24] is used to minimize the gap between the experimental data and the model, allowing the identification of the total thermal resistance of the stack RTH.

V. RESULTS AND DISCUSSION

A. Total thermal resistance RTH

The total thermal resistance of the stack RTH was measured from 50°C to 400°C with a 100°C/min heat rate. Each temperature measurement was realized im-

	$k(T(°C))$ (W/m/K)	ref.
SiN	$4.66e^{-9}T^3 - 5.80e^{-6}T^2 + 2.84e^{-3}T + 1.15$	[18]
Si	$5.23e^{-4}T^2 - 0.451T + 144.3$	Unpublished
GeGST	amorphous state: 0.29 phase transition: $3.4e^{-3}T - 0.3228$ crystalline state: 0.76	[19]
TiN	$4T^{0.29}$	[20]

Table I. Parameters required for the computation of RTH in the amorphous phase from relation (2). References are also indicated for each parameter.

mediately after reaching the setpoint temperature (no lag time) with 12 frequencies ranging from 753 Hz to 5123 Hz. This frequency range allows the heat to penetrate deeper than the stack and the wafer to keep its semi-infinite character. The thermal resistance RTH for the 100 nm MLS (N=5) stack and the 200 nm MLS (N=10) stack are reported in Fig. 3. As expected doubling the MLS thickness increases RTH. There is a linear trend, that is described by equation 3, where N is proportional to the thickness of the MLS. The thermal resistance of a single 100 nm thick GeGST layer (measured in previous works [19]) is also reported in Fig. 3 for comparison. Both GeGST/TiN MLS show higher RTH than the 100 nm thick GeGST sample. This can be explained by the contribution of the multiple interfaces within the MLS and the extra TiN thickness. Moreover, non stabilization of the thermal resistance of the MLS during cooling can be explained by the variation of the thermal conductivity of the TiN which is big enough from room temperature to 450°C to be noticed on RTH. The drop of the thermal resistance noticed between 250-280°C can be attributed to a structural reorganization inside the MLS. However, the magnitude of the thermal resistance drop is unusual (i.e. smaller) compared to previous work [19]. An in-situ structural analysis of the samples from room temperature to 450°C and back to room temperature has been conducted in order to investigate this behavior.

B. In-situ structural analysis

An in-situ Raman scattering analysis was performed from room temperature (RT) to 450 °C using an INVIA Renishaw confocal spectrometer coupled to a Leica optical microscope. Two monochromatic laser excitations were used, namely 532 nm and 785 nm. The temperature of the samples was controlled via a furnace (LINKAM TS 1000) working under an Ar inert atmosphere. The temperature rate was 100 °C/min with a short plateau of about 30 seconds to stabilize temperature before each spectral acquisition. Low level laser power densities i.e. 1% or 5% of the peak-power (100 to 200 mW) were used in order to avoid unwanted additional heating by the incident radiation. The spectrometer is fitted with an edge filter cutting the back-scattered light below ~ 100 cm^{-1}.

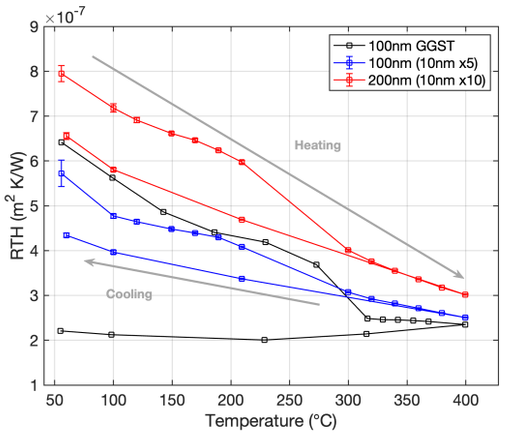

Figure 3. Total thermal resistance of the stack deposited on the silicon wafer for the two different MLS thicknesses and for a 100 nm thick GeGST layer. The heating rate is 100°C/min, each temperature measurement requires 5 minutes. The sample were in the amorphous state before heating.

The spectral resolution of the Stokes-side Raman spectra was ~ 1 cm^{-1}.

At RT, the main feature of the Raman spectrum of the (GST+Ge45% (10nm)/ TiN (10nm))x5 co-sputtered superlattice is a large band spreading over the 100-190 cm^{-1} spectral region (Fig. 4). This band is essentially composed of two overlapping bands centered around 125 cm^{-1} and 150 cm^{-1} that shall be paralleled to the Raman signature of the amorphous GST ($Ge_2Sb_2Te_5$) reference alloy. The band centered at 125 cm^{-1} (Fig. 4) can be connected to vibrations of tetrahedral species of type $GeTe_{4-n}Ge_n$ ($n = 0, 4$) ([25–32])[2] and to Ge-based defective octahedra within the amorphous GeTe compound of the Ge-rich alloy ([32, 34–36]). The larger part of the structure of the amorphous GeTe compound is probably more formed by the latter geometry than by the former tetrahedral Ge ([32, 36]). The band centered at $\sim$ 150 cm^{-1} (Fig. 4) can be ascribed to the stretching mode of amorphous $SbTe_3$ pyramids ([14, 28, 32]) and to defective octahedral coordination of Sb atoms ([32]) and Te atoms ([36]). Vibrating edge-sharing tetrahedra in the amorphous GeTe component may contribute around 160 cm^{-1} to this large band ([31, 37]). A contribution from amorphous Te-Te stretching mode bond vibrations in the GeTe compound ([38–41]) is here improbable ([26, 29, 30, 32, 42]). At higher frequencies ($\sim$ 220 cm^{-1}), the ν_3(F2) antisymmetric stretching mode of tetrahedra in amorphous GeTe ([14, 27, 28, 32, 35, 36]) contributes to a broad bulge over the 190 – 300 cm^{-1} region associated with a-Ge in tetrahedral sites[3] (Fig. 4). Hence, the two local geometries namely the glass tetrahe-

[2] The shoulderat 110 cm^{-1} may also express the Eg2 vibration of Sb-Te bonds e.g. [33].
[3] This bulge is actually formed by two overlapping bands at ∼270

dral environment and the rock-salt defective octahedral geometry coexist in the disordered as-deposited Ge-rich alloy. As expected[4], TiN rock-salt-structured (essentially Raman inactive) encapsulating GeGST sublayers showed a quite weak Raman signature e.g. in the form of a loose bulge distorting at most the baseline around 550 cm^{-1} ([43]).

From RT to 227°C, the Raman spectra remained unchanged.

At 280°C, the relative weight of the band at ∼125 cm^{-1} increased noticeably with respect to SbTe modes (Fig. 4). Such evolution expressed the rearrangement of Ge-Te bonds around more consistent SbTe units. Before addressing the rationale of this evolution, let us first discuss what it does not express: Although an increase of Ge-Te modes has been reported as a distinctive feature of the crystallization of fcc GST ($Ge_2Sb_2Te_5$) ([14, 33]), this did not apply here. Indeed, in amorphous Ge-rich GST, the transition towards fcc GST (as temperature T increases) is a threefold process whereby a mandatory transient phase first appears, which triggers the subsequent nucleation and growth of cubic Ge and GST (the latter forms last) ([13, 14, 33, 44]). In this study, as Ge-Te modes increase, the in-excess a-Ge (expressed by overlapping loose peaks at 220 and 270 cm^{-1}) does not turn into c-Ge state (peaking at ∼ 335 cm^{-1}) (Fig. 4). Therefore, fcc GST cannot be realized. Furthermore, the drop of the thermal resistance accompanying the observed increasing Ge-Te modes is too small (Fig. 3) to be related to the crystallization of GST. Recall also that cubic GST is metastable. Thus, the observed consistency of the Raman spectra (1) over the temperature range of 280°C to 450°C and (2) back to RT (Fig. 4) is another argument in favor of non-formation of crystalline GST. This is to say, if the latter formed at high temperature, it would (at least partially) not sustain back to RT and the respective Raman spectra shall differ more markedly than in Fig. 4. Non-appearance of cubic GST may result from the compressive stress exerted by TiN encapsulation which typically induces a large increase of the crystallization temperature ([45, 46]). Consider now the rationale underlying the increase of Ge-Te modes from 280°C onwards. Recall that thermal diffusion of Ge atoms in GST or Ge-rich GST has been reported in the literature ([47]) to proceed above 220°C via grain boundaries through a polycrystalline layer. Yet, in our opinion, work by Prazakova et al. ([14, 33]) or Rahier et al. ([44]) suggests that Ge diffusion shall also occur in the amorphous state. Indeed, the formation of the above-mentioned neoformed transient crystalline phase namely, GeTe, that mandatorily precedes crystallization of both Ge and GST ([44]) cannot be realized if Ge atoms do not diffuse beforehand in the amorphous material. According to Rahier et al. ([44]), this transient GeTe is thermally activated above 300°C. In this study it would be activated slightly below 300°C and would be responsible for the marked increase of Ge-Te modes at 280°C (Fig. 4). The subsequent (and expected) crystallization of GST is most likely delayed to a higher temperature due to TiN encapsulation ([45]). Thus the neoformed GeTe phase sustains up to 450°C and the Raman spectra remain essentially unchanged. From 280°C onwards, the discrete shift towards lower frequencies (120 cm^{-1}) of GeTe modes is consistent with appearance of crystallized GeTe and may be connected with the Γ_1(A1) mode in crystalline α-GeTe ([32, 48]). In any case, this neoformed GeTe contributes to the (incomplete) evolution of the layers towards the rhombohedrally deformed rock-salt structure. Of course increase of GeTe modes from 280°C onwards may also be partially related to breakage of homopolar bonds e.g. Sb-Sb which promote the 4-coordination for Ge ([26, 29, 30, 34]).

As the Raman analysis suggests, the compressive stress exerted by TiN encapsulation induces a large increase of the crystallization temperature. This increase of the crystallization temperature can explain the unexpected lower drop in RTH (Fig. 3) compared to previous work [19]. In order confirm that the TiN encapsulation might be at the origin of this behavior, we need to make sure that the interfaces between the layers of the MLS are still intact after annealing. Otherwise, the hypothesis would be wrong. Thus, SEM micrographs and ToF-SIMS analysis were realized and are respectively reported in Fig. 5 and Fig. 6. It is shown that the interfaces are still in very good condition even after annealing. The ToF-SIMS analysis shows that the Ge, Sb and Te are confined and do not spread through the TiN layers. This further supports that the TiN layers are exerting compressive stress on the GeGST layers,thereby, increasing the crystallization temperature.

C. GeGST/TiN interfacial thermal resistance

It has been assessed that the interfaces in MLS are well preserved after annealing, which allows their characterization, even after the atomic reorganization . Considering equation (3), after subtracting the SiN layer contribution, it comes:

$$R = N \underbrace{\left(\frac{e_{GeGST}}{k_{GeGST}} + \frac{e_{TiN}}{k_{TiN}} + 2TBR_{GeGST/TiN}\right)}_{R_{cell}} + TCR \quad (7)$$

By doing a linear regression (N being the slope and TCR the intercept), it is possible to estimate the thermal resistance of one unit cell (or period) $R_{cell} = \frac{e_{GeGST}}{k_{GeGST}} + \frac{e_{TiN}}{k_{TiN}} + 2TBR_{GeGST/GST}$ and the sum of the thermal boundary resistances outside the MLS, namely TCR. The two identified quantities are reported in Fig. 7 and Fig. 8 respectively. Considering that the Fourier regime still valid for a thickness of 10 nm, it is possible to sub-

and 220 cm^{-1} assigned to the TO and LO vibrational modes of amorphous Ge, respectively ([14]).

[4] Personal conversation with Georges Chollon (Laboratory LCTS - UMR 5801, Pessac France).

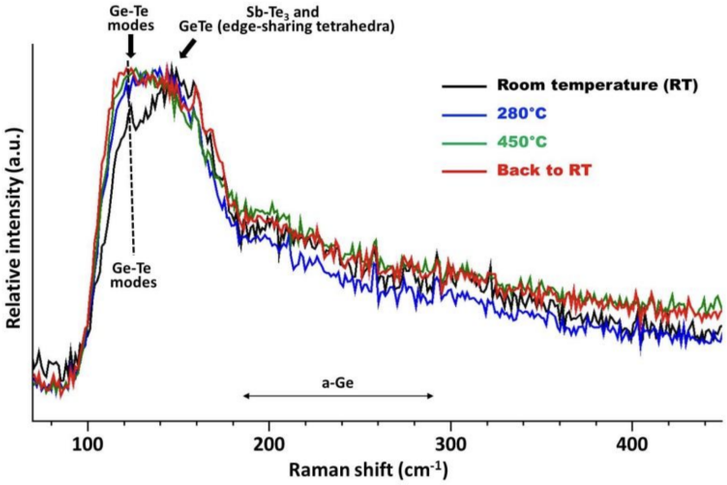

Figure 4. In-situ Raman analysis (laser excitation: 785 nm) of a (GST+Ge45% (10nm)/ TiN (10nm))x5 MLS from room temperature to 450°C. The black spectrum is at room temperature, the blue spectrum is at 280°C , the green spectrum is at 450°C and the red spectrum is after cooling back to room temperature.

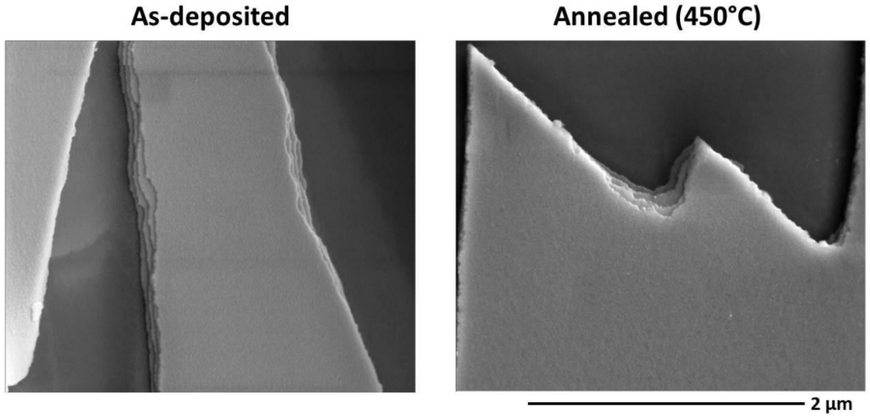

Figure 5. SEM micrographs of a (GST+Ge45% (10nm)/ TiN (10nm))x5 MLS. Left: as-deposited. Right Annealed at high temperature (450°C).

tract the contribution of the GeGST and the TiN layers from the thermal resistance of one unit cell. This leads to the identification of the thermal boundary resistance $TBR_{GeGST/TiN}$ between GeGST and TiN layers.The results are reported in Fig. 9. The sum of the interfacial thermal resistances TCR identified is in good concordance with previous studies. In a work realized by Kusiak et al. [19] it was shown that the sum of the thermal boundary resistances $TCR_{kusiak} = TBR_{Pt/GeGST} + TBR_{GeGST/TiN} + TBR_{SiN/Si}$, identified with their experimental conditions, was ranging from from 1.2×10^{-7} m^{2}K/W to 3.4×10^{-7} m^{2}K/W. Comparing these values to our work, it is observed that $TCR > TCR_{kusiak}$. This is due to the addition of a TiN layer between the Pt and the GeGST that plays the role of an adhesive layer. This adhesive layer was deposited to improve adhesion of platinum on GeGST. This adhesive layer also induces a reduction of TCR of approximately 60%. Regarding $TBR_{GeGST/TiN}$ at low temperatures, in amorphous state, the experimental values are close to the one computed with the DMM. The parameters used in the DMM computation are listed in Table II [49–51]. However, DMM computations at higher temperatures diverge from experimental values. This can be explained by the atomic rearrangements towards the rock-salt structure of the GeGST which itself leads to an increase of the phonon velocities[52]. Ultimately, an increase of the phonon velocities leads to a decrease of the interfacial thermal resistances. It is shown in Fig. 9 that $TRB_{GeGST/TiN}$ decreases when the temperature increases (tending to 0 at high temperatures), thus showing a linear behavior. Since the TiN layers keep the GGST atoms confined, there is no reason that after annealing (back to room temperature), the values of $TBR_{GGST/TiN}$ should be very different from their original values since the interfaces

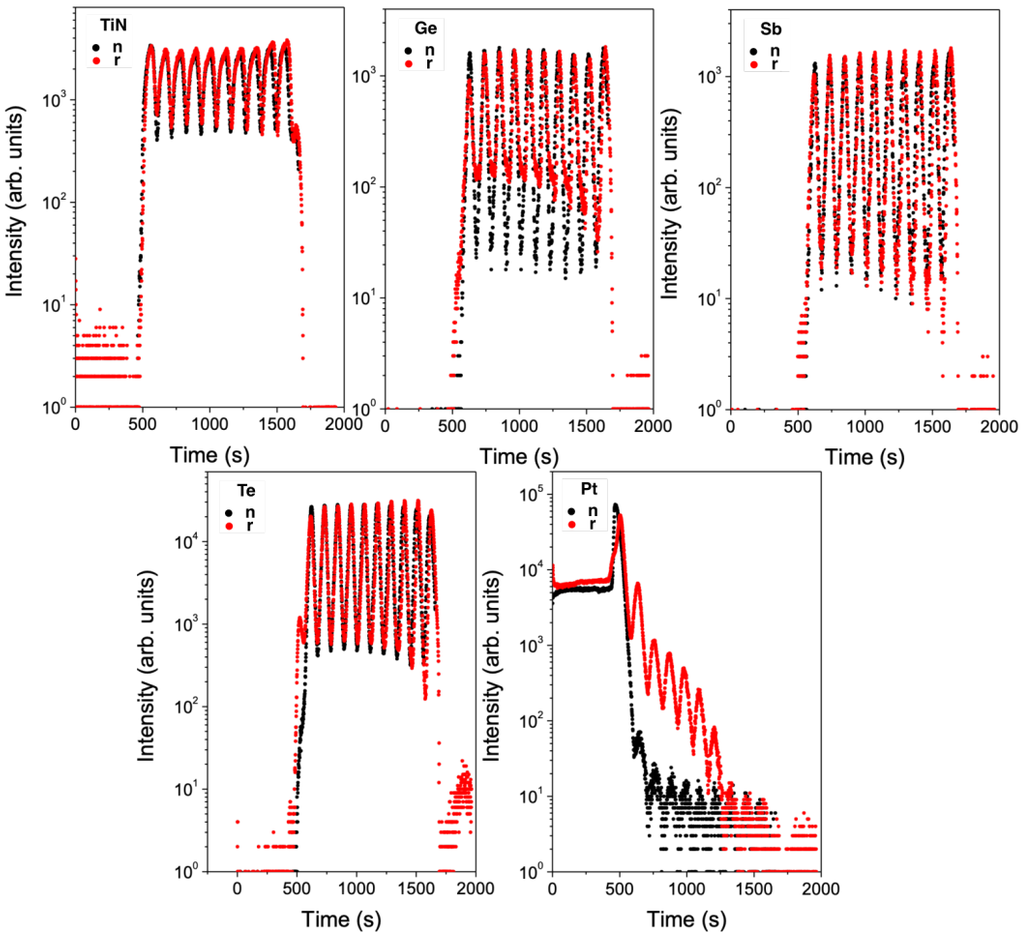

Figure 6. ToF-SIMS measurement realized on the 200 nm thick sample before (black dots) and after annealing at 400°C (red dots).

between layers have not moved. Thus, it is possible to describe $TBR_{GeGST/TiN}$ behavior by a linear fit, following the equation $TBR = -2.7173T + 1.1 \times 10^{-8}$. Such values means that there is little room for improvement regarding the TiN and GeGST contact. The experimental values are indeed close to the DMM computations that represent the minimal interfacial thermal resistance (ideal case) between GeGST and TiN. Moreover, $TBR_{GeGST/TiN}$ tends to zero, meaning that at high temperatures they do not contribute much. To improve PCRAM functioning, thermally speaking, it might be better to try to develop new geometries or even new alloys with new doping. It is possible to note that in Fig. 7 and in Fig. 8 the error bars in the low-temperature region are noticeably smaller than the ones in the high-temperature region. This is due to a difference in the signal amplitude between the two regions. Indeed, for the lower temperature, the signal amplitude is much lower than the one at high temperature, leading to a more accurate estimation of RTH at high temperature. Since the uncertainty for the indentifcation of RTH was propagated to compute R_{cell} and

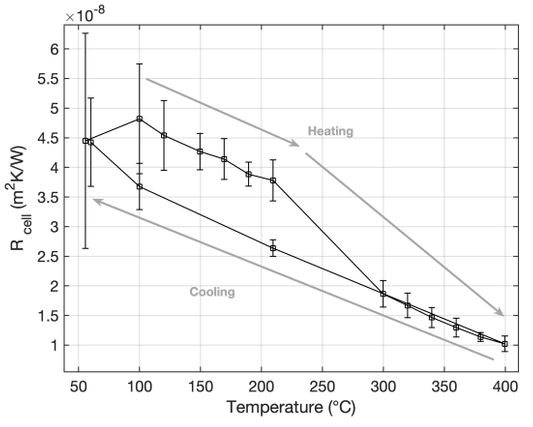

Figure 7. Thermal resistance R_{cell} of a unit cell of the MLS computed by linear regression using equation (7).

TCR uncertainties, it is then normal to observe a similar trend.

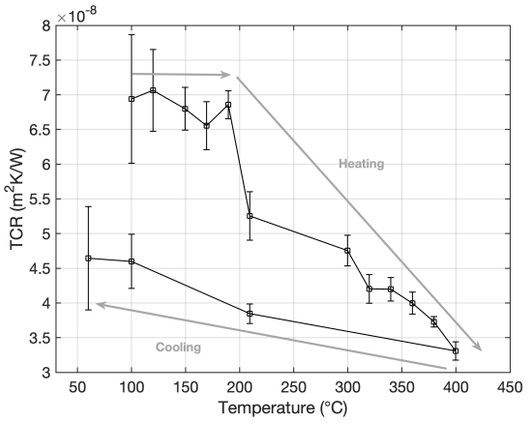

Figure 8. Sum of the interfacial thermal resistances $TCR = TBR_{Pt/TiN} + TBR_{SiN/Si} + TBR_{TiN/SiN}$ from the stack computed by linear regression using equation (7).

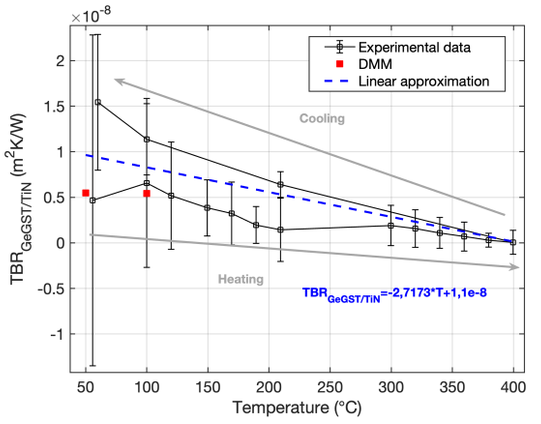

Figure 9. Interfacial thermal resistance $TBR_{GeGST/TiN}$ between GeGST and TiN layers from 50°C to 400°C computed based on the values of R_{cell} (equation (7) and Fig. 7) using the parameters provided in Table I.

VI. CONCLUSION

In this paper the interfacial thermal resistance between GeGST and TiN has been characterized by modulated photothermal radiometry. It was shown that its value tends to zero at high temperatures. A linear approximation of the interfacial thermal resistances was given. The measurements are in good agreement with the literature. Moreover Raman spectroscopy and ToF-SIMS measurement showed that the TiN layers have an influence on the crystallization temperature of the GeGST. This shift of the crystallization temperature is attributed to a compressive stress exerted by the TiN layers on the GeGST layers.

	V_L (m/s)	V_T (m/s)	$\Theta_{D_{th}}$ (K)	ρ (kg/m^3)	M (g/mol)
GGST	3600	2530	2530	6400	110
TiN	10221	5110	580	5210	61,87

Table II. Parameters used for the DMM computation of $TBR_{GeGST/TiN}$ [49–51].

ACKNOWLEDGMENTS

This work has received funding from the European Union Horizon 2020 research and innovation program under Grant Agreement No. 824957 (BeforeHand: Boosting Performance of Phase Change Devices by Hetero- and Nanostructure Material Design).

[1] A Redaelli, Redaelli, and Lekhwani. *Phase Change Memory.* Springer, 2017.

[2] S W Fong, C M Neumann, and H-S P Wong. Phase-change memory. towards a storage-class memory. *IEEE*

Transactions on Electron Devices, 64(11):4374–4385, 2017.

[3] A L Lacaita and A Redaelli. The race of phase change memories to nanoscale storage and applications. *Microelectronic engineering*, 109:351–356, 2013.

[4] X Zhou, M Xia, F Rao, L Wu, X Li, Z Song, S Feng, and H Sun. Understanding phase-change behaviors of carbon-doped Ge2Sb2Te5 for phase-change memory application. *ACS applied materials & interfaces*, 6(16):14207–14214, 2014.

[5] G B Beneventi, L Perniola, V Sousa, E Gourvest, S Maitrejean, JC Bastien, A Bastard, B Hyot, A Fargeix, C Jahan, et al. Carbon-doped gete: a promising material for phase-change memories. *Solid-State Electronics*, 65:197–204, 2011.

[6] S Tyson, G Wicker, T Lowrey, S Hudgens, and K Hunt. Nonvolatile, high density, high performance phase-change memory. In *2000 IEEE Aerospace Conference. Proceedings (Cat. No. 00TH8484)*, volume 5, pages 385–390. IEEE, 2000.

[7] F Pellizzer, A Pirovano, F Ottogalli, M Magistretti, M Scaravaggi, P Zuliani, M Tosi, A Benvenuti, P Besana, S Cadeo, et al. Novel/spl mu/trench phase-change memory cell for embedded and stand-alone non-volatile memory applications. In *Digest of Technical Papers. 2004 Symposium on VLSI Technology, 2004.*, pages 18–19. IEEE, 2004.

[8] B Yu, X Sun, S Ju, D B Janes, and M Meyyappan. Chalcogenide-nanowire-based phase change memory. *IEEE Transactions on Nanotechnology*, 7(4):496–502, 2008.

[9] F Xiong, M Bae, Y Dai, A D Liao, A Behnam, E A Carrion, S Hong, D Ielmini, and E Pop. Self-aligned nanotube–nanowire phase change memory. *Nano letters*, 13(2):464–469, 2013.

[10] M Longo, R Fallica, C Wiemer, O Salicio, M Fanciulli, E Rotunno, and L Lazzarini. Metal organic chemical vapor deposition of phase change Ge1Sb2Te4 nanowires. *Nano letters*, 12(3):1509–1515, 2012.

[11] RE Simpson, P Fons, AV Kolobov, T Fukaya, M Krbal, T Yagi, and J Tominaga. Interfacial phase-change memory. *Nature nanotechnology*, 6(8):501–505, 2011.

[12] J-L Battaglia, A Kusiak, V Schick, A Cappella, C Wiemer, M Longo, and E Varesi. Thermal characterization of the Si02-Ge2Sb2Te5 interface from room temperature up to 400 c. *Journal of Applied Physics*, 107(4):044314, 2010.

[13] V Sousa, G Navarro, N Castellani, M Coue, O Cueto, C Sabbione, P Noe, L Perniola, S Blonkowski, P Zuliani, et al. Operation fundamentals in 12Mb phase change memory based on innovative Ge-rich GST materials featuring high reliability performance. In *2015 Symposium on VLSI Technology (VLSI Technology)*, pages T98–T99. IEEE, 2015.

[14] L Prazakova, E Nolot, E Martinez, F Fillot, D Rouchon, N Rochat, M Bernard, C Sabbione, D Morel, N Bernier, et al. Temperature driven structural evolution of Ge-rich GeSbTe alloys and role of N-doping. *Journal of Applied Physics*, 128(21):215102, 2020.

[15] G Navarro, V Sousa, P Noé, N Castellani, M Coué, J Kluge, A Kiouseloglou, C Sabbione, A Persico, A Roule, et al. N-doping impact in optimized Ge-rich materials based phase-change memory. In *2016 IEEE 8th International Memory Workshop (IMW)*, pages 1–4. IEEE, 2016.

[16] D Maillet and S Andre. J. batsale, a. degiovanni, and c. moyne, thermal quadrupoles, 2000.

[17] A Degiovanni, C Pradere, E Ruffio, and J-L Battaglia. Advanced thermal impedance network for the heat diffusion with sources. *International Journal of Thermal Sciences*, 130:518–524, 2018.

[18] AJ Griffin Jr, FR Brotzen, and PJ Loos. The effective transverse thermal conductivity of amorphous Si3N4 thin films. *Journal of applied physics*, 76(7):4007–4011, 1994.

[19] A Kusiak, C Chassain, A M Canseco, K Ghosh, M-C Cyrille, A L Serra, G Navarro, M Bernard, N-P Tran, and J-L Battaglia. Temperature-dependent thermal conductivity and interfacial resistance of Ge-Rich Ge2Sb2Te5 films and multilayers. *physica status solidi (RRL)–Rapid Research Letters*, 16(4):2100507, 2022.

[20] MW Barsoum, CJ Rawn, T El-Raghy, AT Procopio, WD Porter, H Wang, and CR Hubbard. Thermal properties of Ti 4 AlN 3. *Journal of Applied Physics*, 87(12):8407–8414, 2000.

[21] E T Swartz and R O Pohl. Thermal boundary resistance. *Reviews of modern physics*, 61(3):605, 1989.

[22] DW Mardquardt. An algorithm for least square estimation of parameters. *J. Soc. Ind. Appl. Math*, 11:431–441, 1963.

[23] David D Morrison. Methods for nonlinear least squares problems and convergence proofs. In *JPL SEMINAR PROC. ON TRACKING PROGRAMS AND ORBIT DETERMINATION 26 FEB. 1960*, 1960.

[24] Kenneth Levenberg. A method for the solution of certain non-linear problems in least squares. *Quarterly of applied mathematics*, 2(2):164–168, 1944.

[25] M Först, T Dekorsy, C Trappe, M Laurenzis, H Kurz, and B Béchevet. Phase change in Ge 2 Sb 2 Te 5 films investigated by coherent phonon spectroscopy. *Applied Physics Letters*, 77(13):1964–1966, 2000.

[26] DA Baker, MA Paesler, G Lucovsky, SC Agarwal, and PC Taylor. Application of bond constraint theory to the switchable optical memory material Ge 2 Sb 2 Te 5. *Physical review letters*, 96(25):255501, 2006.

[27] KS Andrikopoulos, SN Yannopoulos, GA Voyiatzis, AV Kolobov, Michel Ribes, and J Tominaga. Raman scattering study of the $a-gete$ structure and possible mechanism for the amorphous to crystal transition. *Journal of physics: condensed matter*, 18(3):965, 2006.

[28] KS Andrikopoulos, SN Yannopoulos, AV Kolobov, P Fons, and J Tominaga. Raman scattering study of GeTe and Ge2Sb2Te5 phase-change materials. *Journal of Physics and Chemistry of Solids*, 68(5-6):1074–1078, 2007.

[29] P Jóvári, I Kaban, J Steiner, B Beuneu, A Schöps, and A Webb. ẃrong bondsín sputtered amorphous Ge2Sb2Te5. *Journal of Physics: Condensed Matter*, 19(33):335212, 2007.

[30] P Jóvári, I Kaban, J Steiner, B Beuneu, A Schöps, and MA Webb. Local order in amorphous Ge 2 Sb 2 Te 5 and Ge Sb 2 Te 4. *Physical Review B*, 77(3):035202, 2008.

[31] R De Bastiani, AM Piro, MG Grimaldi, E Rimini, GA Baratta, and G Strazzulla. Ion irradiation-induced local structural changes in amorphous Ge 2 Sb 2 Te 5 thin film. *Applied Physics Letters*, 92(24):241925, 2008.

[32] P Němec, Virginie Nazabal, Alain Moréac, J Gutwirth, L Beneš, and M Frumar. Amorphous and crystallized Ge–Sb–Te thin films deposited by pulsed laser: Local

structure using raman scattering spectroscopy. *Materials Chemistry and Physics*, 136(2-3):935–941, 2012.

[33] L Prazakova, E Nolot, E Martinez, D Rouchon, F Fillot, N Bernier, R Elizalde, M Bernard, and G Navarro. The effect of ge content on structural evolution of Ge-rich GeSbTe alloys at increasing temperature. *Materialia*, 21:101345, 2022.

[34] S Caravati, M Bernasconi, TD Kühne, M Krack, and M Parrinello. Coexistence of tetrahedral-and octahedral-like sites in amorphous phase change materials. *Applied Physics Letters*, 91(17):171906, 2007.

[35] R Mazzarello, S Caravati, S Angioletti-Uberti, M Bernasconi, and M Parrinello. Erratum: Signature of tetrahedral Ge in the raman spectrum of amorphous phase-change materials [phys. rev. lett. 104, 085503 (2010)]. *Physical Review Letters*, 107(3):039902, 2011.

[36] G C Sosso, S Caravati, R Mazzarello, and M Bernasconi. Raman spectra of cubic and amorphous Ge 2 Sb 2 Te 5 from first principles. *Physical Review B*, 83(13):134201, 2011.

[37] S Sugai. Stochastic random network model in Ge and Si chalcogenide glasses. *Physical Review B*, 35(3):1345, 1987.

[38] J Tominaga and N Atoda. Study of the crystallization of gesbte films by raman spectroscopy. *Japanese journal of applied physics*, 38(3B):L322, 1999.

[39] L Bo, S Zhi-Tang, Z Ting, F Song-Lin, and C Bomy. Raman spectra and xps studies of phase changes in Ge2Sb2Te5 films. *Chinese Physics*, 13(11):1947, 2004.

[40] H Satoh, K Sugawara, and K Tanaka. Nanoscale phase changes in crystalline Ge 2 Sb 2 Te 5 films using scanning probe microscopes. *Journal of Applied Physics*, 99(2):024306, 2006.

[41] S J Park, M H Jang, S-J Park, M-H Cho, and D-H Ko. Characteristics of phase transition and separation in a in–ge–sb–te system. *Applied surface science*, 258(24):9786–9791, 2012.

[42] G Lucovsky, DA Baker, MA Paesler, and JC Phillips. Spectroscopic and electrical detection of intermediate phases and chemical bonding self-organizations in (i) dielectric films for semiconductor devices, and (ii) chalcogenide alloys for optical memory devices. *Journal of non-crystalline solids*, 353(18-21):1713–1722, 2007.

[43] S Grosso. *Revêtements architecturés de Ti, TiN et TiO élaborés par pulvérisation cathodique au défilé sur des fils en acier inoxydable: relation entre la composition chimique, la microstructure et les propriétés d'usage*. PhD thesis, Université Grenoble Alpes, 2017.

[44] E Rahier, S Ran, N Ratel Ramond, S Ma, L Calmels, S Saha, C Mocuta, D Benoit, Y Le Friec, M A Luong, et al. Crystallization of Ge-Rich GeSbTe alloys: The riddle is solved. *ACS Applied Electronic Materials*, 4(6):2682–2688, 2022.

[45] RE Simpson, M Krbal, P Fons, AV Kolobov, J Tominaga, T Uruga, and H Tanida. Toward the ultimate limit of phase change in Ge2Sb2Te5. *Nano letters*, 10(2):414–419, 2010.

[46] A Redaelli. Self-consistent numerical model. *Phase Change Memory: Device Physics, Reliability and Applications*, pages 65–88, 2018.

[47] M A Luong, S Ran, M Bernard, and A Claverie. An experimental study of ge diffusion through Ge2Sb2Te5. *Materials Science in Semiconductor Processing*, 152:107101, 2022.

[48] EF Steigmeier and G Harbeke. Soft phonon mode and ferroelectricity in GeTe. *Solid State Communications*, 8(16):1275–1279, 1970.

[49] K Aryana, J T Gaskins, J Nag, D A Stewart, Z Bai, S Mukhopadhyay, J C Read, D H Olson, E R Hoglund, J M Howe, et al. Interface controlled thermal resistances of ultra-thin chalcogenide-based phase change memory devices. *Nature communications*, 12(1):774, 2021.

[50] SA Baily, David Emin, and Heng Li. Hall mobility of amorphous Ge2Sb2Te5. *Solid state communications*, 139(4):161–164, 2006.

[51] J F Shackelford and W Alexander. *CRC materials science and engineering handbook*. CRC press, 2000.

[52] H-K Lyeo, D G Cahill, B-S Lee, J R Abelson, M-H Kwon, K-B Kim, S G Bishop, and B-K Cheong. Thermal conductivity of phase-change material Ge 2 Sb 2 Te 5. *Applied Physics Letters*, 89(15):151904, 2006.

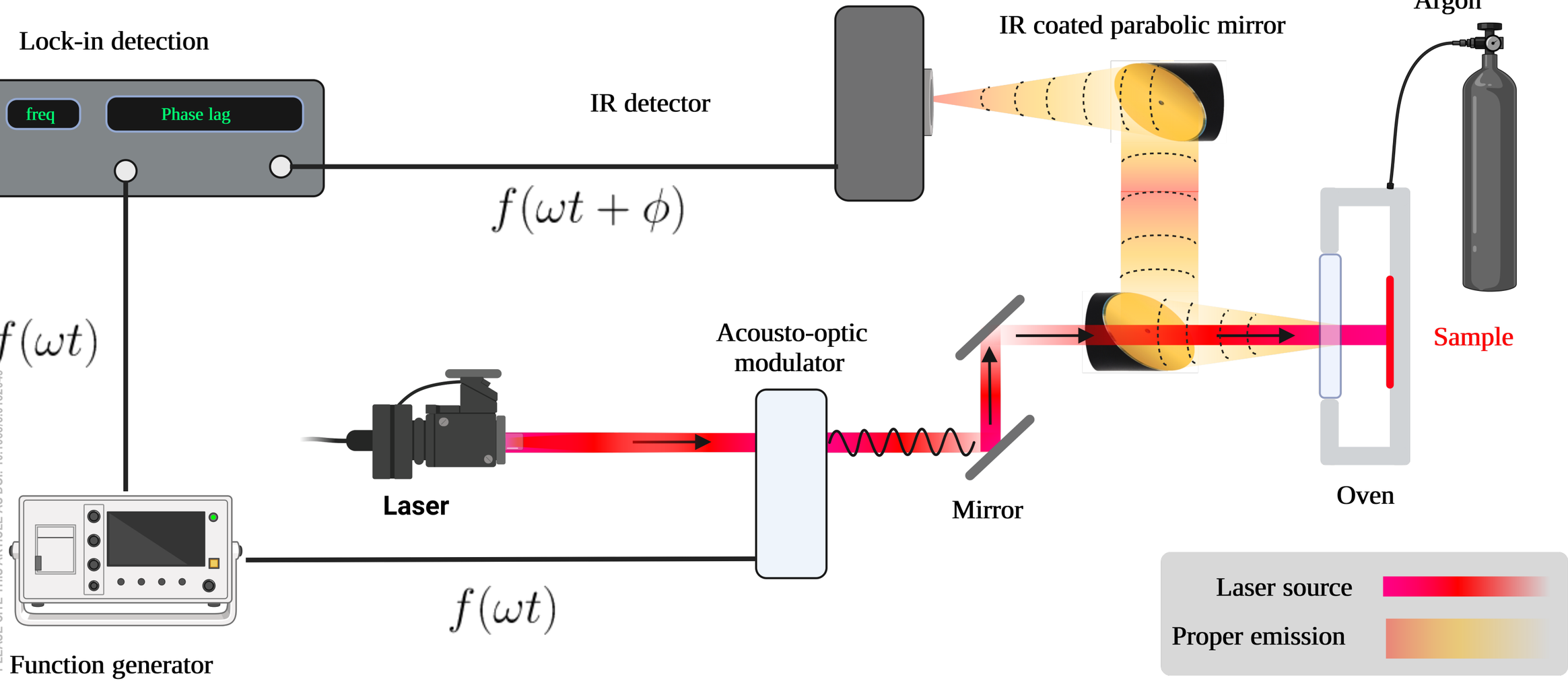

Journal of Applied Physics

AIP Publishing

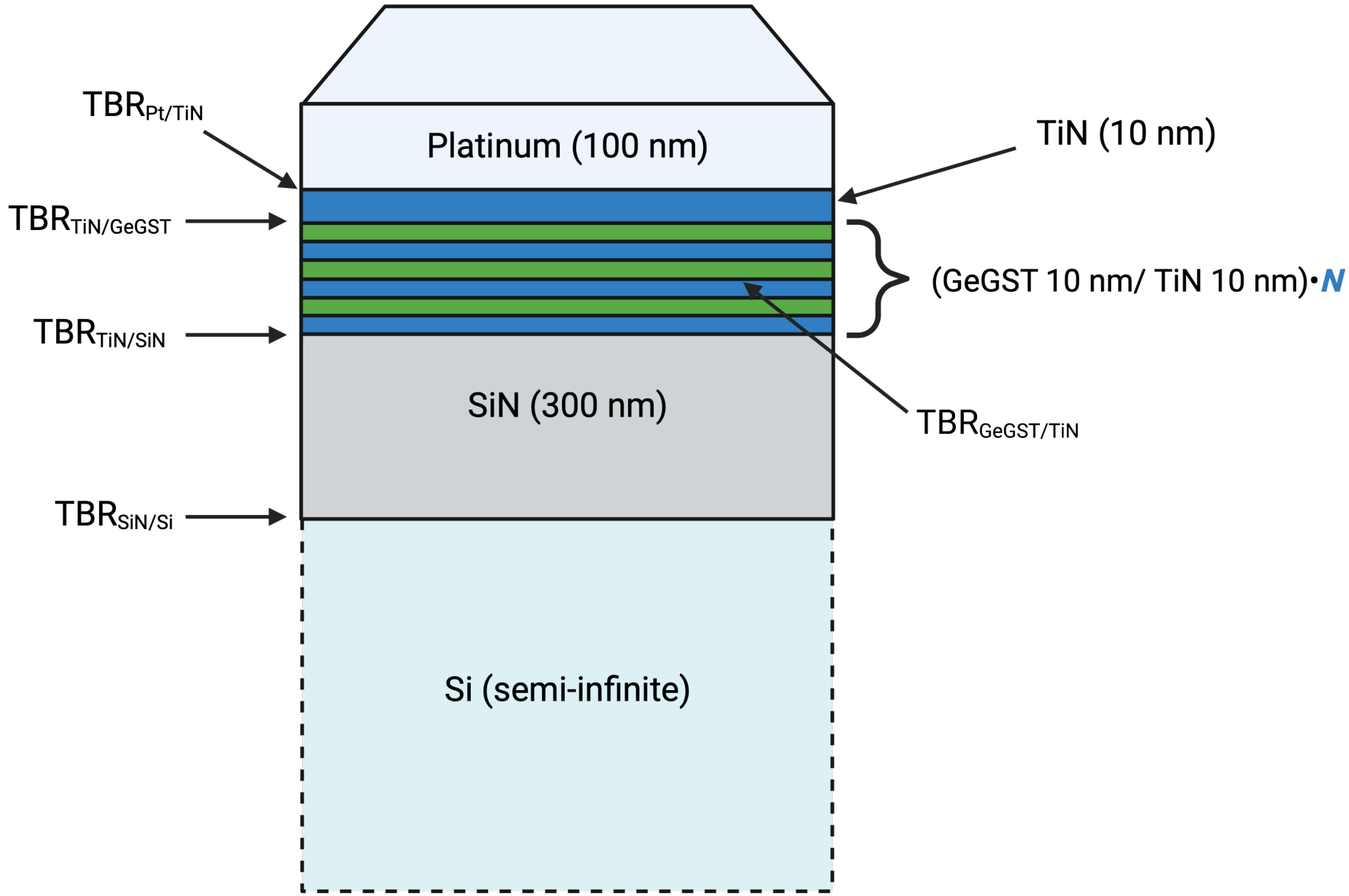

Journal of Applied Physics

AIP Publishing

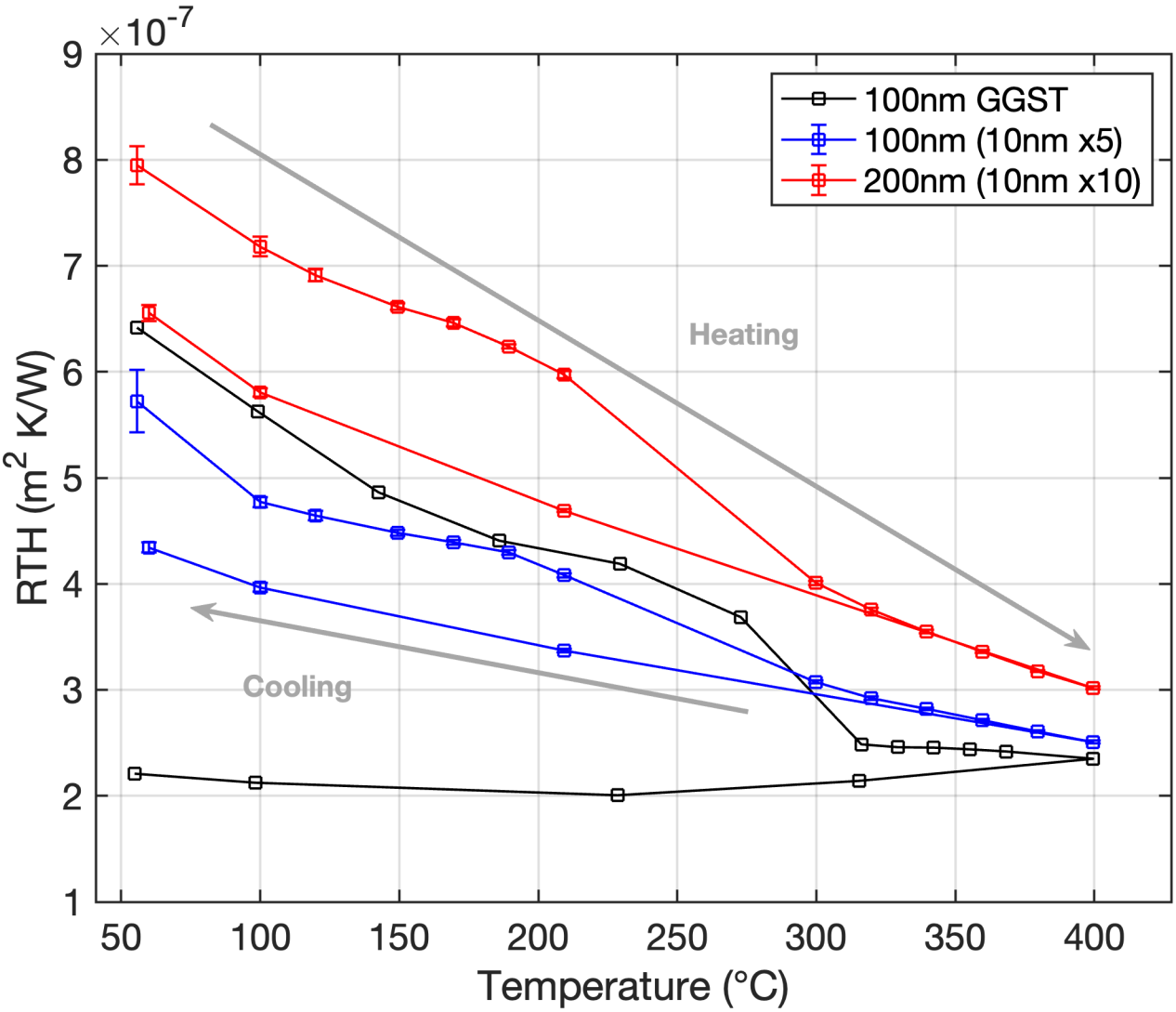

AIP Publishing
Journal of Applied Physics
ACCEPTED MANUSCRIPT

PLEASE CITE THIS ARTICLE AS DOI: 10.1063/5.0132048

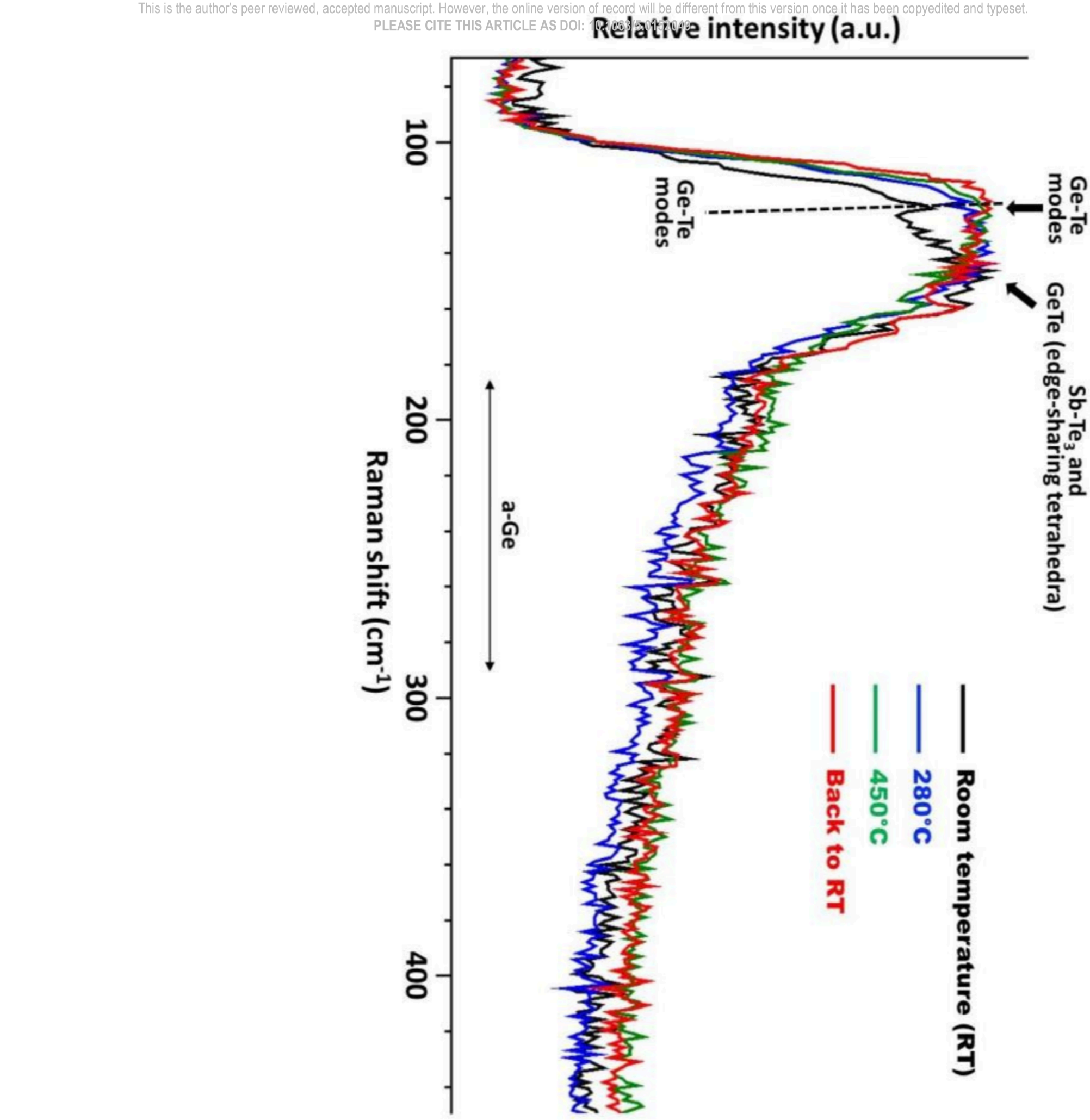

Journal of Applied Physics

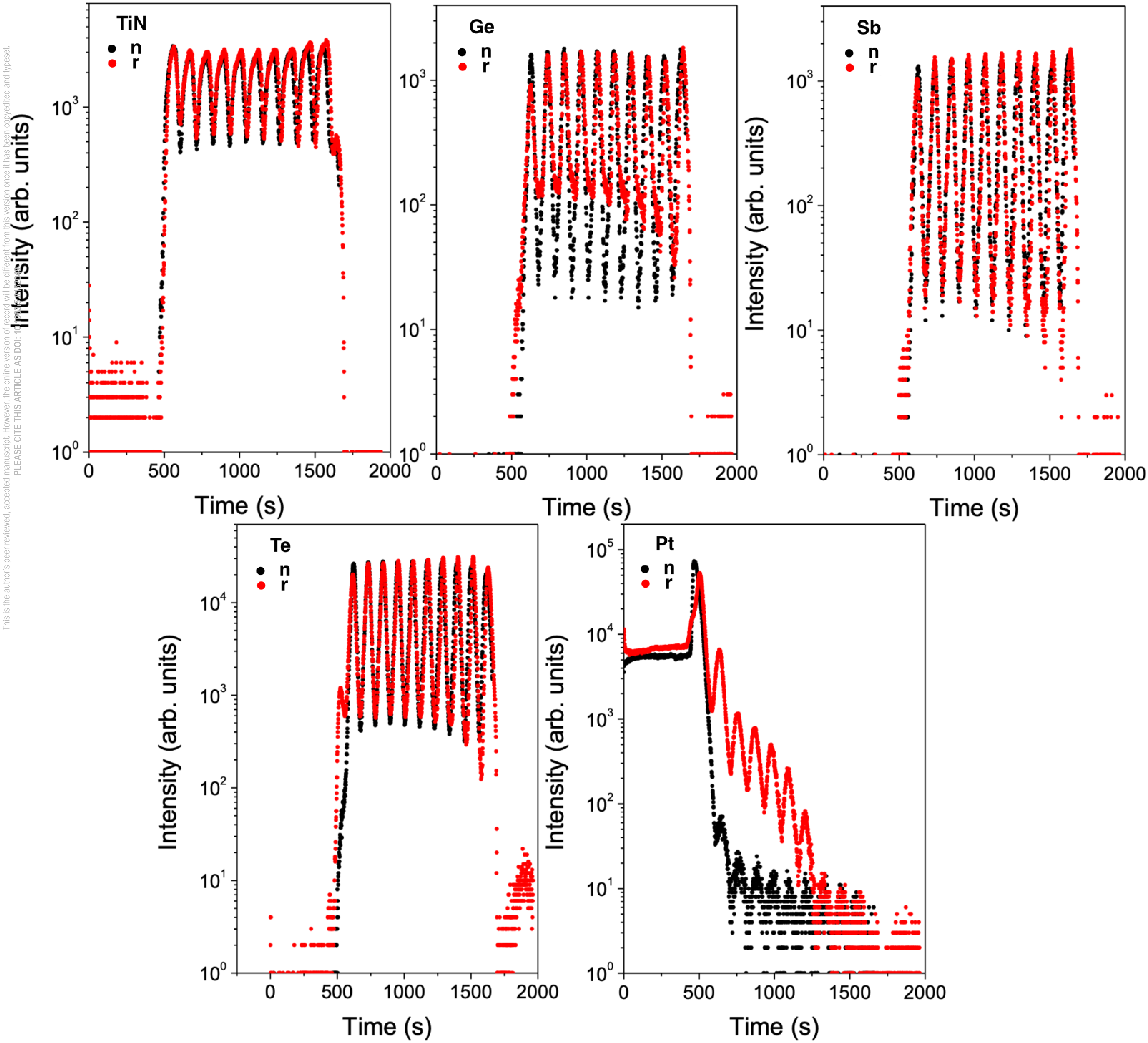

Journal of Applied Physics

AIP Publishing

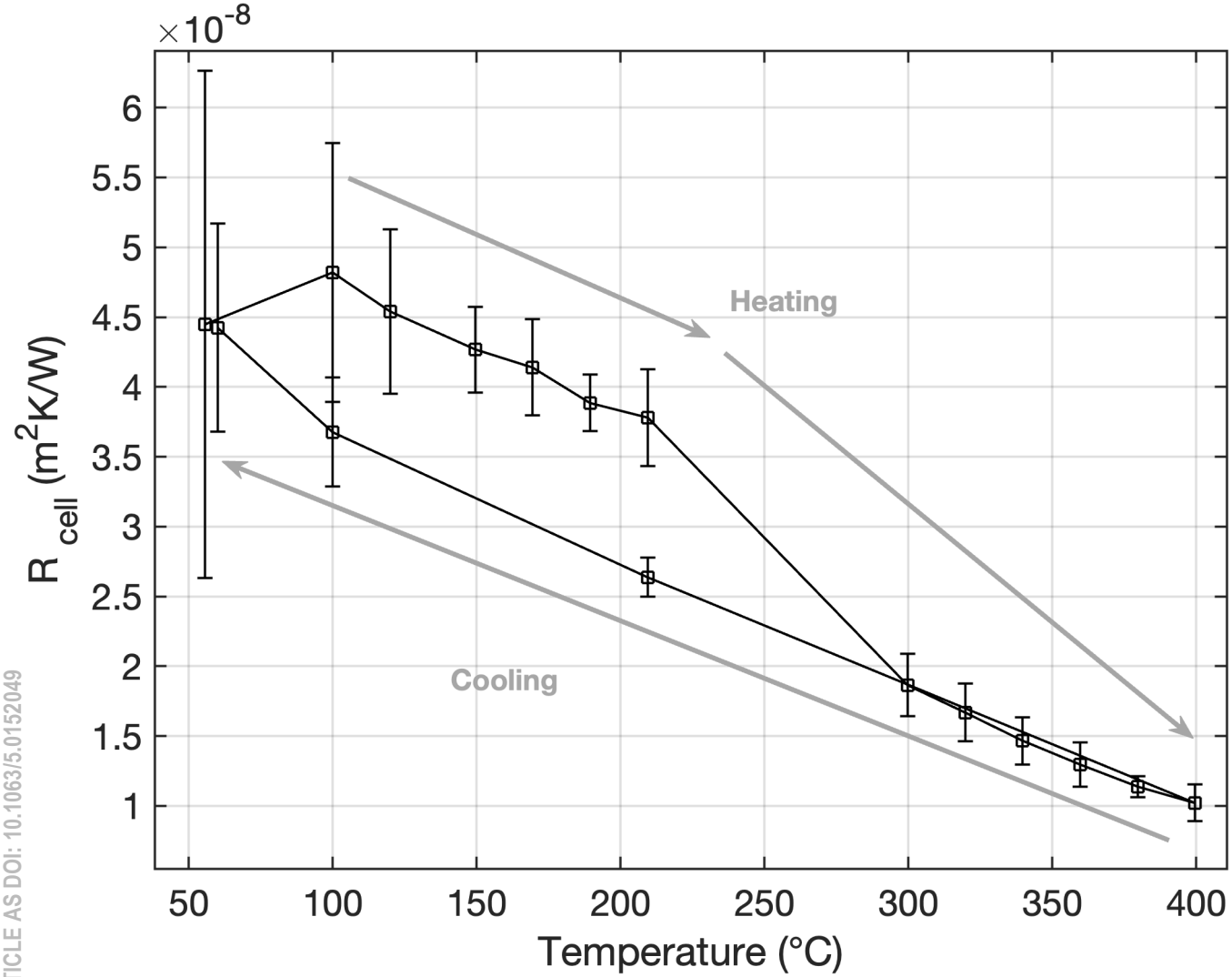

Journal of Applied Physics

AIP Publishing

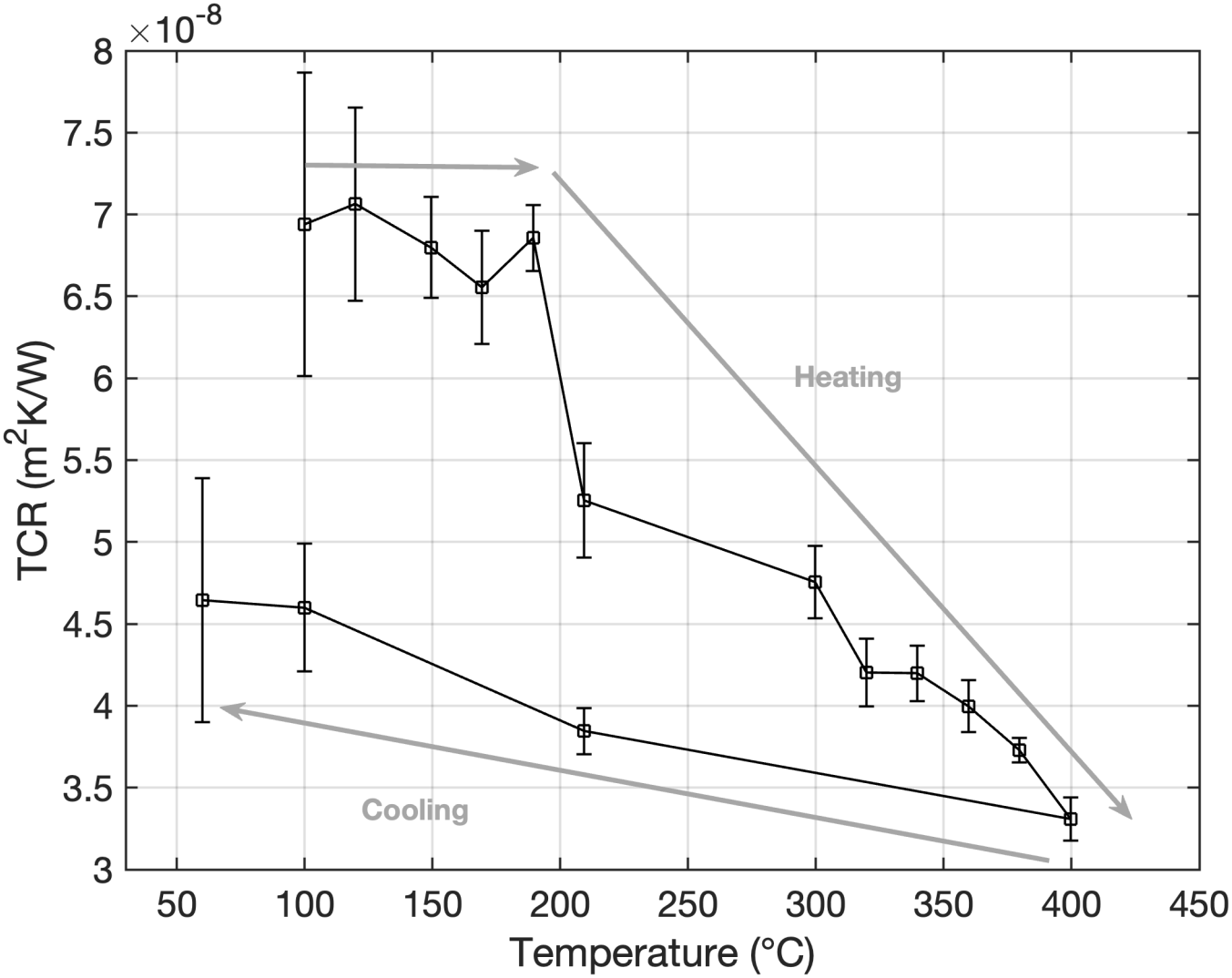

Journal of Applied Physics

AIP Publishing